ELSEVIER

Journal of Pharmaceutical and Biomedical Analysis
22 (2000) 325–339

JOURNAL OF
PHARMACEUTICAL
AND BIOMEDICAL
ANALYSIS

www.elsevier.com/locate/jpba

Analysis of film coating thickness and surface area of pharmaceutical pellets using fluorescence microscopy and image analysis

Martin Andersson [a], Björn Holmquist [b], Jörgen Lindquist [c], Olle Nilsson [a], Karl-Gustav Wahlund [a,*]

[a] *Department of Technical Analytical Chemistry, Centre for Chemistry and Chemical Engineering, Lund University, P.O. Box 124, S-221 00 Lund, Sweden*
[b] *Department of Mathematical Statistics, Lund University, P.O. Box 118, S-221 00 Lund, Sweden*
[c] *Analytical Chemistry, Pharmaceutical R&D, AstraZeneca R&D Mölndal, S-431 83 Mölndal, Sweden*

Received 24 June 1999; received in revised form 1 October 1999; accepted 14 November 1999

Abstract

A method is presented which enables geometrical characterisation of pharmaceutical pellets and their film coating. It provides a high level of details on the single pellet level. Image analysis was used to determine the coating thickness (h) applied on the pellets and the surface area (A) of the pellet cores. Different definitions of A and h are evaluated. Hierarchical analysis of variance was used to resolve different sources contributing to the total variance. The variance within pellets and the variance between pellets were found as significant sources of variation. Special emphasis was put on evaluation of A/h due to its influence on the release rate of an active drug substance from the pellet core. The pellet images were thus used to predict variations in the release rate using a mathematical model as a link between the image data and the release rate. General aspects of image analysis are discussed. The method would be useful in calibration of near infrared spectra to h in process analytical chemistry.

Keywords: Image analysis; Pellets; Coating; Thickness; Surface area; Hierarchical analysis of variance; Release rate

1. Introduction

There is a need to characterise products manufactured within the pharmaceutical industry. These products are usually obtained in a series of operations, one of which is the film coating process. The film coating is applied using a fluidised bed process [1], where pellet cores of 0.1–1 mm in diameter containing the active drug are covered with a permeable membrane, a coating layer. By this, the dissolution after administration of the drug is prolonged, and controlled release can be

* Corresponding author. Tel.: +46-46-2228316; fax: +46-46-2224525.
E-mail address: karl-gustav.wahlund@teknlk.lth.se (K.-G. Wahlund)

0731-7085/00/$ - see front matter
PII: S0731-7085(99)00289-7

obtained. The release rate of the active drug is influenced by many factors. Important ones are the thickness of the coating applied (h) and the surface area (A) of the pellets [1]. The release rate is high for pellets having thin h and large A, and low for pellets with thicker h and smaller A [1]. Thus, the characterisation of the product in terms of A and h can serve to optimise the process in which the coated pellets are produced.

The mass of the coating applied can be used as an indirect measure of h and A. It can thus be used to predict the release rate [2] of the active drug. Another indirect method, based on assuming perfect spheres and using experimentally determined densities and mass measurements of the coating for a sample of pellets, can be used to reveal both the average h and average A of the pellets [3]. Moreover, the release rate as a function of the specific area can be obtained indirectly from sieve analysis [4–7].

Image analysis [8,9] could enable a direct measurement of h but has so far been concerned mostly with particle size and roundness parameters [1,10–13]. These are determined from images obtained by scanning electron microscopy or cameras facilitated with magnification using, e.g. a visible light microscope, all in order to study the influence of the geometrical parameters upon the release rate. Kanerva et al. [14,15] compared the results from image analysis and laser light diffraction methods to the results obtained from sieve analysis for both spherical particles and differently shaped particles. Image analysis was concluded to be the optimal method for narrow size distributions. The two methods gave similar results and enabled the size distribution of pellets to be determined. With image analysis, pellet shape parameters could also be studied.

For direct determination of h on pharmaceuticals, only a few examples have been presented so far. Moussa et al. [16–18] studied the increase in gel thickness of tablets in water at 37°C using a light transmission image analysis system. After given time intervals, the tablet was removed and frozen in liquid nitrogen, sliced along its axial direction and the increase in gel thickness could be studied along the radial direction. Wesdyk et al. [19,20] studied h on pellets sliced into two sections. The pellets were photographed using a scanning electron microscope, the average film thickness was determined, however only from three measurements, and its influence on the release rate was evaluated. It should be noted that the image analysis technique is of general character and can be found in a wide area of applications, e.g. material technology [21–26] medical science [27–31], and membrane science [32,33], to mention a few.

The objective of this study was to develop image analysis methods for determination of h and A. The latter can be used to predict variations in the release rate using its dependence on variations in A/h. In addition, methods for studying individual segments of the pellet core surface and their association with the corresponding h were developed. To the best of our knowledge no such work has yet been presented. The study was performed on a large number of pellets (394) and a large number of thickness measurements within each pellet (100), enabling statistical analysis of the results. The method described can provide with information on specific sources of variation such as the homogeneity within pellets and between pellets within a batch. Notably, h as well as A can be defined in many different ways, especially in the case of non-ideal geometry, here non-perfect spheres. Details on this was another important aim for the study while in previous studies the definitions were often not given, but instead the image analysis system and its software were referred to. A further objective was to develop a method that would be suitable for calibrating near infrared spectra to h. This would be used for in-line process analytical chemistry of the coating process [34].

2. Experimental

2.1. Materials

Pellet cores containing the active drug substance were manufactured in-house and sieved to a diameter of ca. 400–500 μm. The shape was approximately spherical with a ratio of maximum to minimum radius in the range of 1.1–1.8 for

95% of the pellets. The coating material was ethyl cellulose applied as a solution in ethanol. For each batch experiment ≈ 10 kg of pellet cores was used in which dry air ($< 10\%$ RH) was used for fluidising the pellet bed. Different manufacturing conditions were considered where each experiment was performed in a pilot-scale process equipment. Samples were taken from each batch at ≈ 75, 100 and 125% of the empirical target amount of coating solution added. Each batch was thus run longer than needed, putting the real target amount of coating in the centre of the study.

2.2. Sample preparation

From each sample taken out from a batch, 12 pellets were examined utilising a method similar to that presented by Wesdyk et al. [19]. Each pellet was glued onto a black anodised $15 \times 15 \times 1$ mm iron plate. The glue was smeared out to a thin layer to ensure that only the bottom of the pellet was fixed to the glue. The pellets were bisected using an in-house constructed equipment with a vertical rotating axis and a table with variable height position. Each iron plate, with its attached pellet, was placed on a horizontal magnetic disc fixed on top of the rotating axis. With the axis rotating, the iron plate was slid on the magnet until the pellet was in the centre of rotation. The height position of the table was adjusted to ensure that the pellet would be cut in its equator. This was accomplished by performing the cutting underneath a stereo light microscope, and consequently the height position of the cutting blade could be comprehended and the cutting was performed in the midplane. During rotation at ≈ 10 s per revolution, each pellet was carefully cut by manually pushing a Microtome blade into the pellet. The blade was slid on the table, making the cutting operation steady and stable, and it was noted that the shape of the pellets were not affected by the cutting. This procedure was repeated for 33 samples, totalling $33 \times 12 = 396$ pellets.

2.3. Image examination

After being cut, each pellet was photographed using a camera coupled to an incident light fluorescence microscope (Fig. 1A). This took advantage of the fact that the core and the coating showed fluorescence but with different intensities. The colour images were stored on a Kodak Photo CD and converted to bitmap files, readable for the Matlab Image Processing Toolbox. With a macro routine, the inner and outer borders of the coating were marked at 20–30 points using the computer mouse, to define the respective borders (Fig. 1B). At places were the borders were changing in a more curved manner, the points were chosen closer to each other, to capture the overall curvature. The points of the inner and outer border, respectively, were connected using an interpolating parametric cubic spline curve, implemented in Matlab Spline Toolbox (Fig. 1C). The two borders were stored as vectors, containing ≈ 2000 points, respectively. The inner border was split into segments of the perimeter defined by equidistant points along it. For each of these segments the corresponding thickness were measured. Thus, a thickness vector for each pellet, consisting of 100 elements was obtained. The thickness of each pellet could hence be regarded as a population of thickness rather than a single thickness value (Fig. 1D). All distances in the images were converted to micrometers using a scaling factor. This scaling factor was obtained with the accuracy of the 1-mm ruler used, which can be considered very good. The precision in the conversion factor was determined to be $\approx 0.07\%$ in relative S.D. A total of 100 points positioned at equal distances along the curve representing the inner border were chosen and different definitions of thickness and area were used. From the already examined pellets, eleven of these were randomly chosen to be studied again after 6 months to get an estimate of the repeatability of the method.

2.4. Definitions of coating thickness

Three different definitions of h were evaluated. One of them was based on the minimum distances from the inner border to the outer border. The second definition was based on the distances from the inner border to the outer border, forced to be locally perpendicular to the inner border. In the third definition, the distances between the bor-

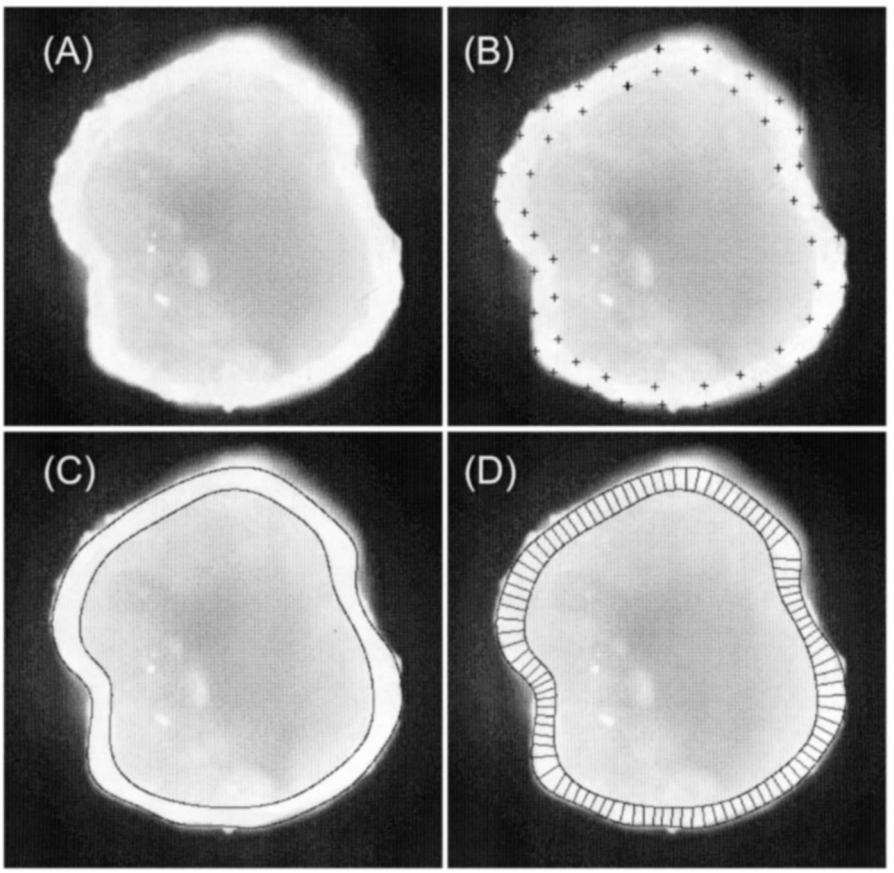

Fig. 1. Fluorescence microscopy image of a coated pellet (A), cut in two halves. The brighter section shows the thin film coating on the core (dark inner section) that contains the active drug substance. The manually marked points (B) are connected using an interpolating parametric cubic spline curve (C). One hundred individual measures of h (D) reflect the distribution of h. Here the minimum distances from the inner border to the outer border are shown.

ders, required to be an extension of the radii originating from the centre of gravity of the pellet, were used.

2.5. Definitions of pellet core segment surface area

Three different models for determination of A_i of the pellet core segments shown in Fig. 2 were defined. The cutting plane of the pellets is here referred to as the equatorial plane and accordingly, the poles of the pellet will be found perpendicular to the equatorial plane.

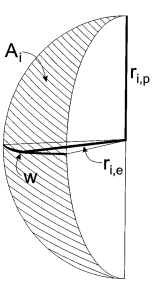

Fig. 2. A_i of a pellet core. The measured segment width in the cutting plane, w, is shown together with the measured equatorial radius, $r_{i,e}$, and the estimated radius to the poles, $r_{i,p}$.

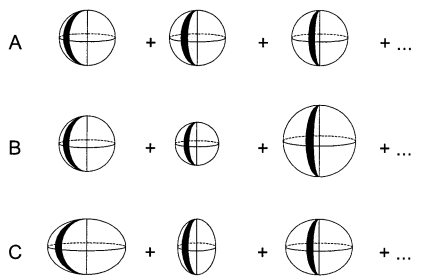

Fig. 3. Illustration of the different models for A. (A) Surface area model 1. All segment areas are of equal size (black sections) based on the average equatorial radius. (B) Surface area model 2 with differently sized segments based on only the equatorial radius for that segment. (C) Surface area model 3 using ellipsoids to describe each of the segments. See Section 2.5 for details.

2.5.1. Surface area model 1

This model was based on assuming that each pellet core could be described by a perfect sphere (Fig. 3A). All the 100 segments around the pellet were assumed to be equally large, 1/100 of total A of the pellet core

$$A_i = \tfrac{1}{100} 4\pi \bar{r}^2_{\text{core}} \tag{1}$$

The pellet core average radius was determined as the mean of all the individual segment radii in the equatorial plane, $\bar{r}_{\text{core}} = \frac{1}{100} \Sigma_{j=1}^{100} r_{j,\text{e}}$.

2.5.2. Surface area model 2

In the second model, the segments of the pellet core are assumed to be sliced out from perfect spheres of different sizes (Fig. 3B). In each of the 100 segments, A_i is assumed to be 1/100 of a sphere with the radius $r_{i,\text{e}}$,

$$A_i = \tfrac{1}{100} 4\pi \bar{r}^2_{i,\text{e}} \tag{2}$$

Consequently, each individual pellet core segment is assumed to have the same polar radius as equatorial radius, i.e. $r_{i,\text{p}} = r_{i,\text{e}}$ for each individual segment (Fig. 2). In general, the area segments within a pellet will not be equally large, and the segments will not coincide in the poles.

2.5.3. Surface area model 3

A more rigorous model is one where A_i is approximated by a segment with the width, w, sliced out from an ellipsoid where w is estimated as a fraction (1/100) of the pellet core perimeter. The segment surface area is then

$$A_i = \begin{cases} w\left(r^2_{i,\text{e}} + \dfrac{r_{i,\text{e}} r^2_{i,\text{p}}\ \arccosh\left(\dfrac{r_{i,\text{e}}}{r_{i,\text{p}}}\right)}{\sqrt{r^2_{i,\text{e}} - r^2_{i,\text{p}}}}\right), & r_{i,\text{e}} > r_{i,\text{p}} \\ w r^2_{i,\text{e}}, & r_{i,\text{e}} = r_{i,\text{p}} \\ w\left(r^2_{i,\text{e}} + \dfrac{r_{i,\text{e}} r^2_{i,\text{p}}\ \arcsin\left(\dfrac{\sqrt{r^2_{i,\text{p}} - r^2_{i,\text{e}}}}{r_{i,\text{p}}}\right)}{\sqrt{r^2_{i,\text{p}} - r^2_{i,\text{e}}}}\right), & r_{i,\text{e}} < r_{i,\text{p}} \end{cases} \tag{3}$$

where $r_{i,\text{e}}$ and $r_{i,\text{p}}$ denote the principal semi-axes of the ellipsoid, based on a circular equator with the radius $r_{i,\text{e}}$. Hence, two of the semi-axes will be equal to $r_{i,\text{e}}$ for the ellipsoid which is used to obtain A_i of that pellet core segment. The polar radius was defined as $r_{i,\text{p}} = \frac{1}{100} \Sigma_{j=1}^{100} r_{j,\text{e}}$ and used for all of the segments within a pellet.

In general, all of the segments will coincide in the poles and A_i of the segments within a pellet will not be equally large (Fig. 3C).

2.6. Ratio of pellet core surface area to coating thickness

By using the definitions of h and A_i, each individual A_i can be associated with its corresponding thickness measurement, h_i to determine A_i/h_i for individual segments. In order to limit the study of individual A_i/h_i, the three different models for A_i were used, but for h_i, the minimum distance was used only.

2.7. Hierarchical analysis of variances

The variances of h on pellets and A/h were examined using hierarchical analysis of variance [35], to enable evaluation of different types of variances, at different levels of detail. Hierarchical analysis of variance can be performed when the structure of the data is nested which was the case here. The analysis is based on the fact that the

total variance can be written as a sum of several variances,

$$\sigma^2_{\text{total}} = \sigma^2_1 + \sigma^2_2 + \sigma^2_3 + \sigma^2_4 + \sigma^2_5 \quad (4)$$

where σ^2_i denote statistically independent variances. These are determined from experimental variances obtained as deviations around the mean value at the level i, $\sigma^2_{i,\text{exp}}$. The individual variances were σ^2_1 = variance between batches, estimated from $\sigma^2_{1,\text{exp}} - \sigma^2_{2,\text{exp}}$, σ^2_2 = variance between samples taken at 75, 100 and 125% of the target processing time (within any batch), estimated from $\sigma^2_{2,\text{exp}} - \sigma^2_{3,\text{exp}}$, σ^2_3 = variance between pellets (within any sample, within any batch), estimated from $\sigma^2_{3,\text{exp}} - \sigma^2_{4,\text{exp}}$, σ^2_4, variance between different positions around the pellet (within any pellet, within any sample,…), estimated from $\sigma^2_{4,\text{exp}} - \sigma^2_{5,\text{exp}}$, and σ^2_5 = variance between replicate measurements (within any position around the pellet, within any pellet,…) = $\sigma^2_{5,\text{exp}}$. The individual variances were calculated in a step-wise procedure. The deviation around the average of replicate measurements would give $\sigma^2_5 = \sigma^2_{5,\text{exp}}$, and further on, the deviation of measurements at different places around their mean would give $\sigma^2_{4,\text{exp}}$. The estimation of σ^2_4 could then be obtained from the subtraction, $\sigma^2_{4,\text{exp}} - \sigma^2_{5,\text{exp}}$. The remaining statistically independent variances were obtained accordingly.

The hierarchical analysis of variance, i.e. the estimation of the statistically independent σ^2_1 through σ^2_5, was numerically performed using Matlab. Standard statistical packages do not usually contain routines for hierarchical analysis of variance when the data set is unbalanced and very large, as was the case here.

3. Results and discussion

The results obtained from image analysis were used to characterise h on the pellets. They also provided possibilities to predict the influence of the geometrical parameters on the release rate. This was enabled by a hierarchical analysis of variance which also gave a detailed description of the variations in the pellets such as variation within pellets and variation between pellets.

3.1. Image analysis

The outer border of the pellet coating was in general easier to determine than the inner border. This was due to the difference in intensities and colours being greater at the outer border where the pellet coating had a strong intensity as opposed to the generally black background. At the inner border the coating was usually only slightly higher in intensity and slightly different in colour from the core, but a little different in texture. The absolute intensities and colours of the coating varied both within pellets and between pellets. The problem of determining whether or not a pixel in the image belonged to the coating, the core, or none of them was thus far from trivial and could not be based on intensities and colours only. A fully automatic, computerised analysis of the images would thus be very complex and a computer program was considered taking too long time to implement, if ever possible.

Instead a manual method was developed. By using manual marking of the borders, artefacts like dust and reflections became manually filtered, and pattern characteristics of the image objects, hard to define mathematically, could be taken into account. The manual markings in the images using the computer mouse started at a point where the border was clearly visible and therefore easy to determine, and then points were marked all around the pellet (Fig. 1B).

The part of the border passing through the manually marked points needed to be constructed by interpolation using curve fitting to the marked points. An interpolating cubic spline curve gave satisfactory agreement with the visible border (Fig. 1C). It was therefore used for the final documentation, and other techniques that were investigated such as interpolations in the polar domain are not discussed here.

The examined distance measures differed mostly where the curvature of the border was strong, especially in regions of convex curvature, and where the h variation was locally strong. The three different approaches used for definition of thickness are illustrated in Fig. 4. They resulted in distributions that were differently skewed, as can be seen in Table 1, where the skewness is indi-

cated by the large deviations from the average to the maximum thickness. The most useful definition of the thickness would be the minimum distance from a point at the inner border to a point at the outer border because the diffusion rate is here maximal and thus dominates the release rate.

The definition of A_i, based on the parameters shown in Fig. 2, was also found to be non-trivial, because it could be based on a population of radii, the mean radius, or the mean of the surface associated to each of the radii. The area measures were more sensitive to the choice of definition than the thickness measurements were. This can be seen when data in

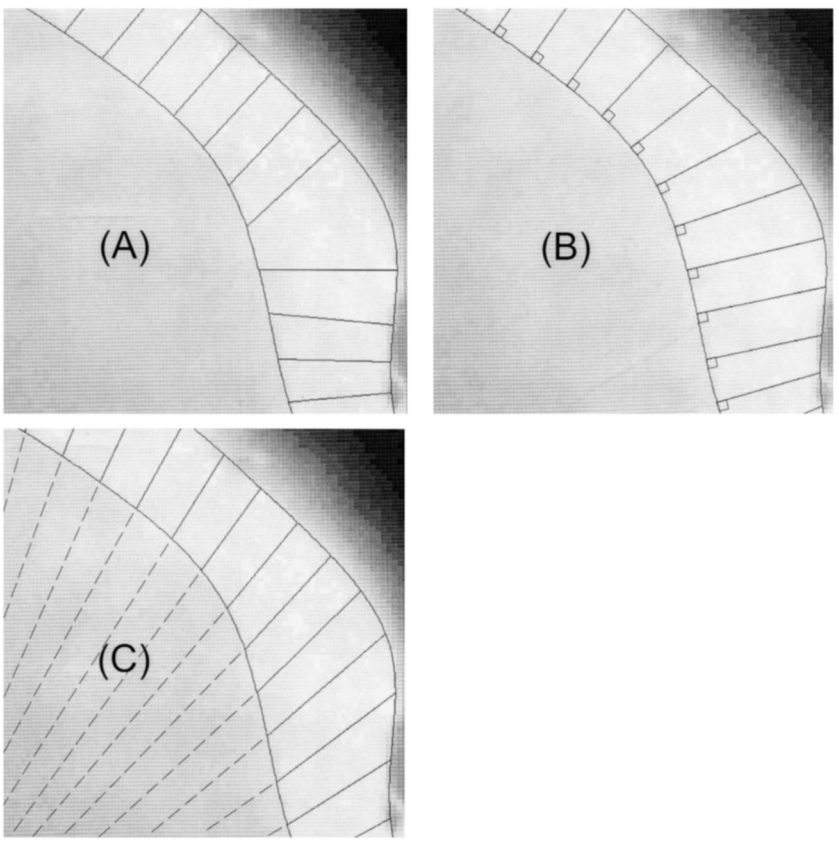

Fig. 4. The different definitions of h. Minimum distance (A), locally perpendicular (B), and extension of the radius from the centre of gravity (C). The sub-images are from the upper right corner of the images of Fig. 1.

Table 1
Comparison of h obtained from the different thickness definitions[a]

Definition	Thickness (h) $\pm$ 95% C.I./μm		
	Minimum ($N = 1$)	Maximum ($N = 1$)	Average ($N = 89$)
Minimum distance	21 ± 4	80 ± 4	44.6 ± 0.6
Locally perpendicular	21 ± 4	96 ± 4	45.1 ± 0.6
Radius extension	21 ± 4	85 ± 4	46.2 ± 0.6

[a] 100% coating applied.

Table 2
Comparison of A of the pellet core obtained from different segment surface area models

Segment surface area model	Individual segment surface area, $A_i \pm 95\%$ C.I./(10^3 μm^2)		$A \pm 95\%$ C.I./(10^3 μm^2)
	Minimum[a] ($N = 1$)	Maximum[a] ($N = 1$)	Total sum ($N = 389$)
1	4.3 ± 0.1	10.9 ± 0.1	718.4 ± 0.5
2	1.4 ± 0.2	16.9 ± 0.2	688.0 ± 0.5
3	4.2 ± 0.1	11.1 ± 0.1	701.2 ± 0.5

[a] Individual segments.

Table 2 are compared with data in Table 1. An important factor in this comparison is that calculations of A include square terms of the individual radii in the equatorial plane.

3.2. Hierarchical analysis of variance

For an ideal homogeneous manufacturing of perfectly spherical pellets with equal sizes and a measurement method for h with no error or random variation, all variance would be found in σ_2^2, i.e. the variance between samples taken out at different processing times (Eq. (4)). There would be no variance between batches, between pellets, between measurements nor between replicate measurements. The reason for the non-zero variance of σ_2^2 is, of course, that it covers the systematic change in thickness during manufacturing. Obviously, as demonstrated in Fig. 1, the ideal situation is not existing and hierarchical analysis of variance was performed in order to quantitate the different variances contributing to the total variance. The total variance was split into the separate components mentioned above, but some confounding still remained, e.g. the variation caused by not cutting exactly in the equator of the pellet. This variation would be a part of σ_3^2 using this hierarchical model. Still, it should be noted that it is not sure that optimal release properties come with ideal, homogeneous geometry.

The different thickness variances obtained from Eq. (4) were calculated and their estimates are presented in Table 3. The 95% confidence limits were also calculated. During calculation, the distributions were evaluated using normal-plots, showing the distributions around the averages at the different levels. The distributions of the h appeared to be close to normally distributed, Fig. 6, except for some of the extreme values. Since the individual values of σ_i were estimated from differences between the experimentally obtained $\sigma_{i,\mathrm{exp}}$, it is obvious that σ_1 is small. $\sigma_{1,\mathrm{exp}}$ and $\sigma_{2,\mathrm{exp}}$ appear as practically identical. However, due to the few replicates at that level, the confidence interval becomes large.

A closer examination of the normal plots reveals that the thickness distributions are slightly asymmetrical (Fig. 5) and have a slight skewness towards large values compared to what would be expected if they were normally distributed. Since σ_2^2 is dependent on the process time interval, it would be of interest to see if it is dependent on the thickness. And, indeed, the plot in Fig. 6 shows that $\sigma_{2,\mathrm{exp}}^2$ increases with the average h for samples taken out at different processing times corresponding to 75, 100 and 125% of the empirical target amount. This is in close agreement with what was obtained by Wnukowski et al. for a similar type of process [36]. It means that if, instead, the hierarchical analysis was based on thickness-corrected variances, σ_i^2/h_i, the σ_2^2/h contribution would become less important. This may be corrected for by using a square root transformation of the individual thickness values [37]. Here, however, the range of thickness for different

Table 3
Standard deviation of thickness[a]

σ_1/μm	σ_2/μm	σ_3/μm	σ_4/μm	σ_5/μm
	7.9	5.1	5.4	3.8
[0–7.9]	[2.5–12.0]	[4.6–5.6]	[4.8–5.9]	[3.7–4.1]

[a] Numbers within brackets are the 95% confidence intervals.

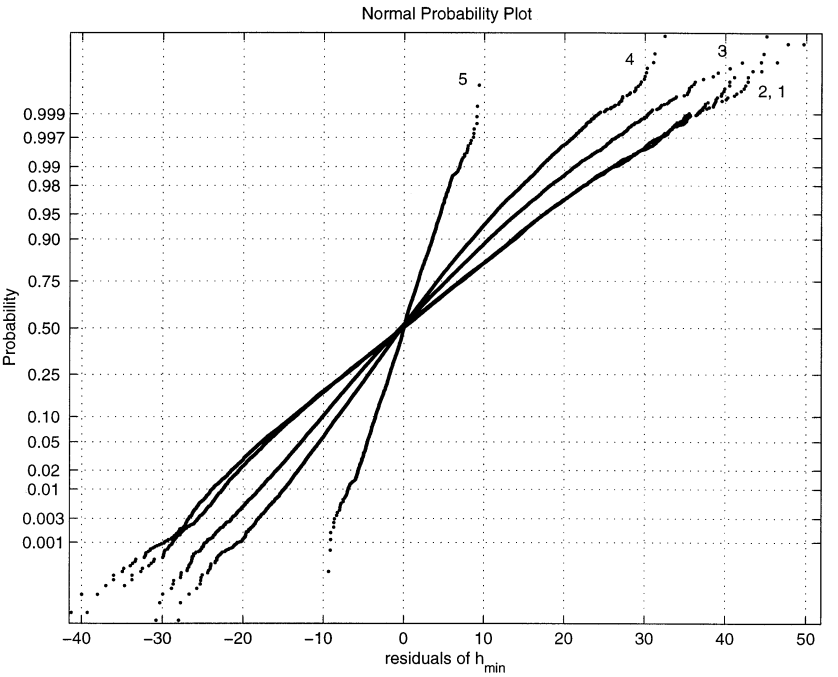

Fig. 5. Deviations of minimum h around average values. Traces 1–5 represent the levels in the hierarchical model. Residual = 0 denotes the average value for each level. From these deviations, $\sigma_{i,\exp}$ were determined, see text for details.

degrees of coating is rather restricted, see Fig. 6, and the effect of such transformation would hence be quite limited. Still, without any thickness correction, the obtained σ_2^2 will represent some average of variation depending on the process time interval. This average will closely represent σ_2^2 at the 100% degree of coating.

The repeatability in the marking of the border was tested for by repeating the marking of the inner and outer borders in eleven of the already examined images after six months. Of course, the curves defining the inner and outer borders, became slightly different. These differences were mostly due to difficulties in determining the borders of the diffuse parts, at some parts resulting in a border inside, and at other parts resulting in a border outside the border first drawn, in a random manner. This repeatability is found in the hierarchical structure and is denoted σ_5^2.

The precision of the conversion factor from pixel-units to micrometers was determined from repeated measurements using a 1-mm ruler. This suggested that the variance caused by imprecision in the scaling factor was negligible, and therefore it was not taken into account for further analysis. However, it would be possible to extend the hierarchical model with another level.

3.3. Predicted influence on the release rate

Since the pellets studied are intended for controlled release formulations, their variation in release rate was evaluated from their geometrical properties. The release rate is depending on A/h, usually included as a proportionality factor regardless of the order of the model. A simple model, assuming zero-order release rate may be described by

$$Q_0 = \frac{A}{h} C_s K_d D_m \tag{5}$$

where Q_0 is the zero-order release rate, C_s is the solubility of the drug substance, K_d is the partition coefficient of the drug substance to the coating and D_m is the diffusion coefficient of the drug substance in the coating. Assuming zero order

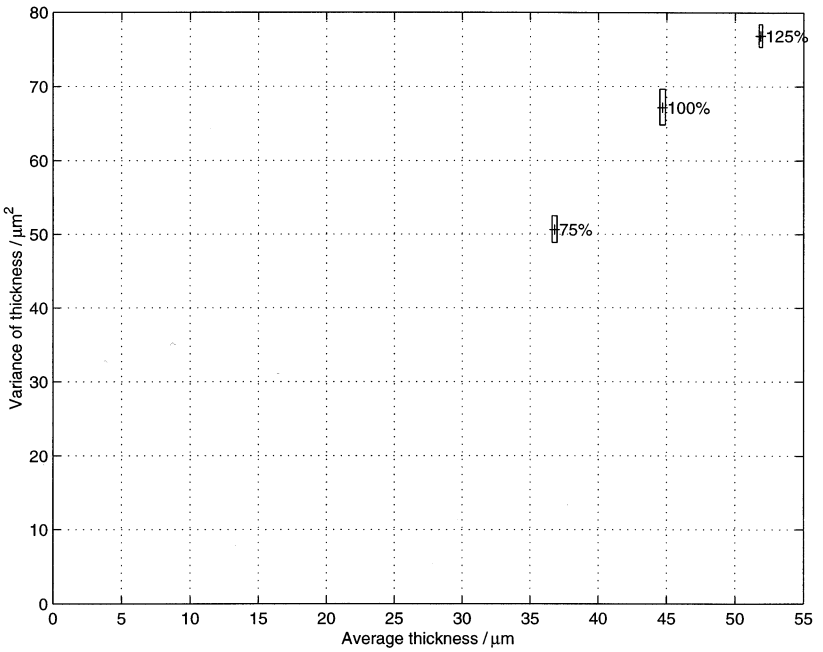

Fig. 6. Variance of thickness, $\sigma^2_{2,\mathrm{exp}}$, plotted as a function of the average thickness. The pellets were taken out at 75, 100 and 125% of the empirical target amount of coating. The width and the height of the boxes indicate the 95% confidence intervals of the average thickness and variance, respectively.

release rate, and that C_s, K_d and D_m are constants, the model can be simplified to

$$Q_0 = \text{constant}\,\frac{A}{h} \tag{6}$$

Thus, the variation of the release rate would be determined by the variation in A/h which is influenced by variations in A as well as h. It is obvious, for example, that segments of large A_i and small h_i will increase the release rate. In Eq. (6), A is an average of the inner and the outer area of the coating. If h is increasing, A will also increase but at a much slower rate, and in order to simplify the calculations, only the inner area was used for predictions of the release rate. Here, surface area model 3 was used together with the minimum distance to determine individual A/h-values. It should be noted that Eq. (6) is not really valid throughout the dissolution process of the drug, because the area and thickness will change when the pellets become wetted. The wetting may simultaneously increase both A and h. This makes it difficult to predict the change in A/h. Still, if A/h is assumed to change with the same factor for all pellets during wetting, this factor will end up as a common change in the constant of Eq. (6). Regarding this, methods to determine the swelling using image analysis are available [16–18].

The analysis of variance for the A/h-values was made analogously to the thickness analysis described above. The major difference was, however, that the distributions of A/h appeared to be log-normal, rather than normal, Fig. 7, as was the case when measuring thickness, Fig. 5. Therefore, to simplify the interpretation of the results, the whole data set with individual A_i/h_i measurements, was log-transformed. Still, after this transformation a curvature remained in the normal plots. For the largest A_i/h_i-values, the logarithmic transformation was not enough. However, the slight skewness will not interfere with any of the results and conclusions made here. After the transformation, the analysis of variance was done in the same way as for the thickness. In order to limit the presentation, only area segment model 3 (Table 4) is used here together with the minimum

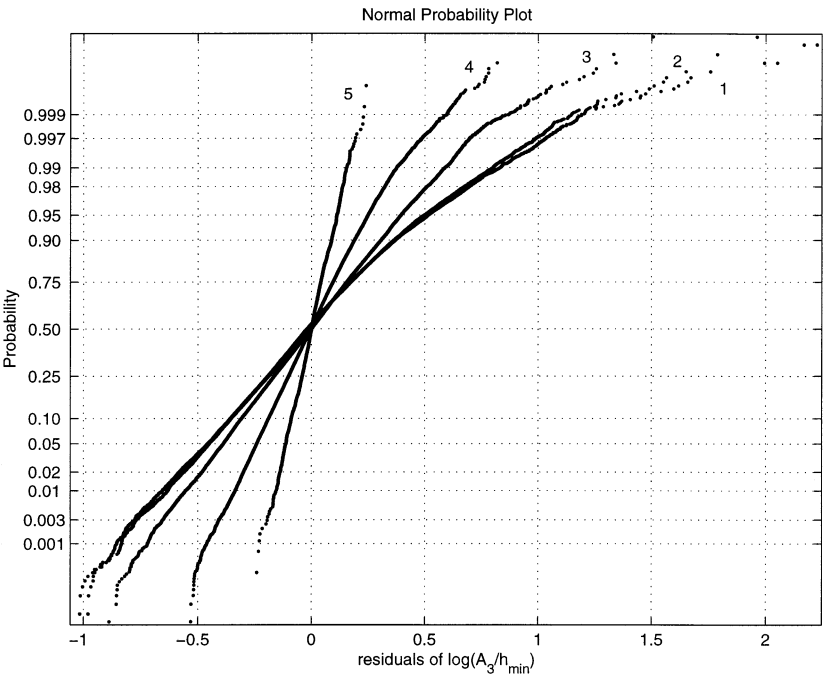

Fig. 7. Deviations of the $\log(A_i/h_i)$ around their average values. Traces 1–5 represent the levels in the hierarchical model. Residual = 0 denotes the average value for all levels. From these deviations, $\sigma_{i,\exp}$ were determined.

Table 4
Comparison of $\log(A_i/h_i)$ obtained from different segment A_i definitions using the minimum thickness as h_i[a]

Segment surface area model	$\log(A/h_{min}) \pm 95\%$ C.I.		
	Minimum[b] ($N=1$)	Maximum[b] ($N=1$)	Mean[b] ($N=89$)
1	4.3 ± 0.1	5.9 ± 0.1	5.06 ± 0.01
2	3.9 ± 0.2	6.1 ± 0.2	5.00 ± 0.01
3	4.7 ± 0.1	5.4 ± 0.1	5.05 ± 0.01

[a] 100% coating applied.
[b] Individual segments.

Table 5
Standard deviation of $\log(A/h)$[a]

σ_1	σ_2	σ_3	σ_4	σ_5
	0.18	0.20	0.13	0.096
[0–0.25]	[0.04–0.3]	[0.18–0.21]	[0.12–0.14]	[0.091–0.101]

[a] Numbers within brackets are the 95% confidence intervals.

thickness. In Table 4 it can be seen that independently of the definition chosen, they end up with quite similar results for the average values. The results from the hierarchical analysis of variance of $\log(A_i/h_i)$ are presented in Table 5. From these results, one can conclude that a significant source of variation in the data came from variation between the pellets, σ_3^2, and also within the pellets, σ_4^2. The inhomogeneity of the raw material in terms of non-ideal geometry, was thus found as a significant source of variation. The hierarchical analysis of variance of $\log(A_i/h_i)$ gave very similar results for all of the area models studied, except for model 2. Thus, for levels l, 2, 3 and 5, in Eq. (4), any of the models can be used, but at level 4 (variance within pellets) the choice of model has a significant role. The variance at level 4 was significantly smaller for the area models l and 3. To find out which model is the most accurate, further experiments are needed, e.g. by slicing the pellets in more than two sections and using methods from stereology.

For all models, the variance between pellets (level 3) were practically the same, ranging from $\sigma_3 = 0.19$ to 0.20. The variance, σ_{CR}^2, that is connected to an average of $\log(A/h)_{pellet}$ of any sample examined for controlled release profiles can be estimated from the variance of $\log(A/h)$ between pellets, σ_3^2, divided by the number of pellets, n, in the sample,

$$\sigma_{CR}^2 = \frac{\sigma_3^2}{n} \tag{7}$$

This is because the observed release rate of a sample is depending on the sum of n individual $\log(A/h)_{pellet}$ contributions having the variance σ_3^2. Hence, the mean release rate in a sample of n pellets has the variance σ_3^2/n.

Since the log-transformed data were close to normally distributed and the data set was very large, about 95% of the expected variation of $\log(A/h)$ for any sample containing n pellets, would be covered by the interval

$$\log(A/h) = \mu_3 \pm 2\sqrt{\frac{\sigma_3^2}{n}} \tag{8}$$

where μ_3 represents the expectation value of $\log(A/h)$ at level 3. Eq. (8) could also be applied

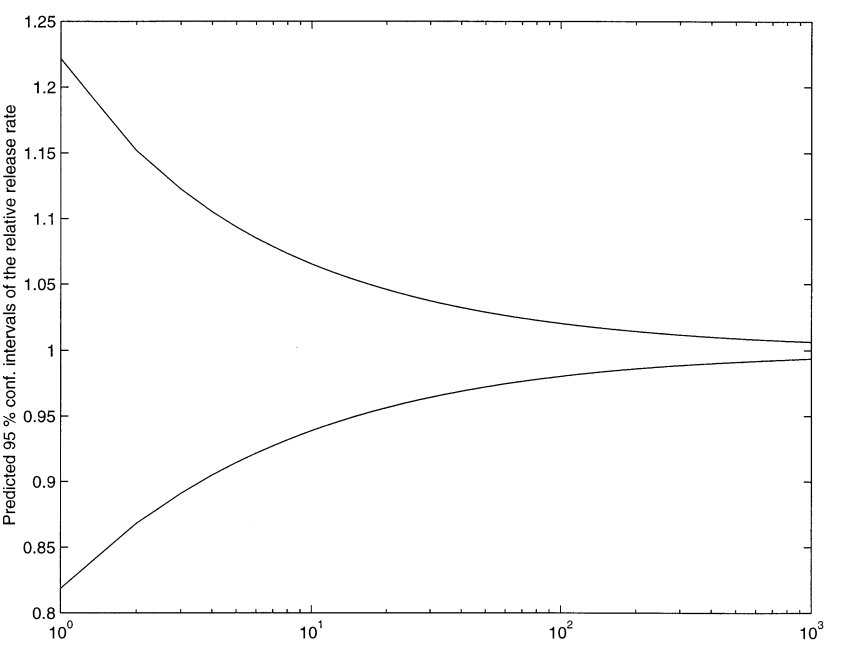

Fig. 8. Predicted confidence intervals for the relative release rate as a function of the number pellets. The upper and lower limits were obtained using Eq. (10).

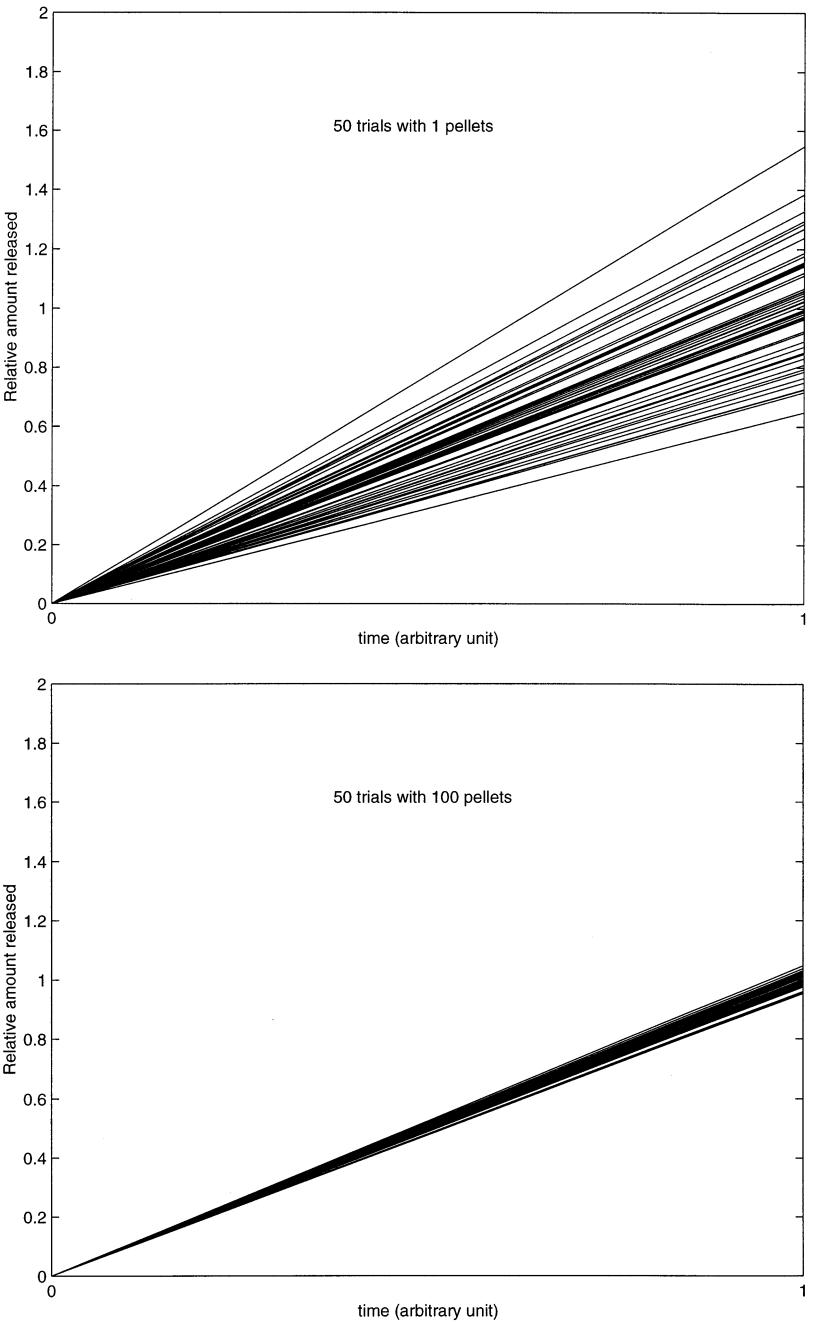

Fig. 9. Simulation of release rate for 50 trials with one pellet (A) and 50 trials with 100 pellets (B). The simulated curves were obtained using Eq. (10) and normally distributed random numbers.

to this investigation, but to get a relevant picture of how the variances were affecting the release rate, the results were inversely transformed, using the exponential function. To reflect the variation of the release rate around the mean value for different numbers of pellets, an interval with a confidence level of 95% would be

$$A/h = e^{\mu_3 \pm \frac{2\sigma_3}{\sqrt{n}}} = e^{\mu_3 \pm \frac{0.40}{\sqrt{n}}} \quad (9)$$

and this interval is obviously non-symmetric. As an alternative to this, the release rate, constant A/h, may be related to the average release rate to obtain a relative release rate $(A/h)_{rel}$ by dividing Eq. (9) with e^{μ}_3, yielding

$$\left(\frac{A}{h}\right)_{rel} = \frac{e^{\mu_3 \pm \frac{2\sigma_3}{\sqrt{n}}}}{e^{\mu_3}} = e^{\pm \frac{2\sigma_3}{\sqrt{n}}} = e^{\pm \frac{0.40}{\sqrt{n}}} \quad (10)$$

Eq. (10) could be plotted for different n which is shown in Fig. 8. It is obvious that the variation diminished rapidly as the number of pellets was increased. The variation becomes more symmetric for large values of n. The interval is below $\pm 2\%$ for $n \geq 400$, and even smaller for the number of pellets, $\approx 10^3$, used in a relevant dose for the material studied here.

As an alternative, the variation of different release rates could be illustrated when employing simulations for different number of pellets, using Eq. (10) and normally distributed random numbers for σ_3. Such simulations are shown in Fig. 9A and B, drawn in the same scaling using arbitrary units, and it is obvious that geometrical variations influence variations in the release rate. Of course, when real dissolution tests are performed, a larger variance can be expected due to further sources of variation, such as non-ideal zero-order dissolution, variations in coating density, coating porosity, and when considering different types of coating. In addition, variations are introduced in the dissolution experiments.

4. Conclusions

The image analysis method can be used to reveal details and characteristics of the material such as variations of h within pellets and between pellets. The quality of the pellets can be determined at different levels of detail using hierarchical analysis of variance. In addition, the image analysis data can be used to predict the variations in release rate due to geometrical variations in the pellets.

The method presented can further be used as a reference method for calibrating near infrared reflectance spectra to h, which can then be used as a quick and non-destructive in-line process analytical chemical method for determination of h [34]. Knowledge of both the average h, and its variance are then very helpful parameters in order to calibrate and to characterise these measurements.

Acknowledgements

Mats O. Johansson, AstraZeneca R&D Mölndal, is acknowledged for experimental support and Jörgen Vessman and Staffan Folestad, AstraZeneca R&D Mölndal, for scientific discussion concerning pharmaceutical analytical chemistry. This work was made possible with support from Astra Hässle AB.

References

[1] G. Ragnarsson, M.O. Johansson, Drug Dev. Ind. Pharm. 14 (1988) 2285–2297.
[2] Z.M. Mathir, C.M. Dangor, T. Govender, D.J. Chetty, J. Microencapsul. 14 (1997) 743–751.
[3] R. Senjokovic, J. Jalsenjak, J. Pharm. Pharmacol. 33 (1981) 279–282.
[4] Y. Fukumori, H. Ichikawa, Y. Yamaoka, E. Akaho, Y. Takeuchi, T. Fukuda, R. Kanamori, Y. Osako, Chem. Pharm. Bull. 39 (1991) 1806–1812.
[5] H. Ichikawa, Y. Fukumori, C.M. Adeyeye, Int. J. Pharm. 156 (1997) 39–48.
[6] G.F. Palmieri, P. Wehrle, Drug Dev. Ind. Pharm. 23 (1997) 1069–1077.
[7] S.P. Li, G.N. Mehta, J.D. Buehler, W.M. Grim, R.J. Harwood, Drug Dev. Ind. Pharm. 14 (1988) 573–585.
[8] R.C. Gonzales, R.E. Woods, Digital Image Processing, Addison-Wesley, Reading, MA, 1992.
[9] C.A. Glasbey, G.W. Horgan, Image Analysis for the Biological Sciences, Wiley, Chichester, 1994.
[10] P.B. Deasy, M.F.L. Law, Int. J. Pharm. 148 (1997) 201–209.

[11] M.P. Gouldson, P.B. Deasy, J. Microencapsul. 14 (1997) 137–153.
[12] H. Lindner, P. Kleinebudde, J. Pharm. Pharmacol. 46 (1994) 2–7.
[13] G. Ragnarsson, A. Sandberg, M.O. Johansson, B. Lindstedt, J. Sjögren, Int. J. Pharm. 79 (1992) 223–232.
[14] H. Kanerva, J. Kiesevaara, E. Muttonen, J. Yliruusi, Pharm. Ind. 55 (1993) 775–779.
[15] H. Kanerva, J. Kiesevaara, E. Muttonen, J. Ylirnusi, Pharm. Ind. 55 (1993) 849–853.
[16] I.S. Moussa, L.H. Cartilier, J. Control. Release 42 (1996) 47–55.
[17] I.S. Moussa, V. Lanaerts, L.H. Cartilier, J. Control. Release 52 (1998) 63–70.
[18] V. Lenaerts, I. Moussa, Y. Dumoulin, F. Mebsout, F. Chouinard, P. Szabo, M.A. Mateescu, L. Cartilier, R. Marchessault, J. Control. Release 53 (1998) 225–234.
[19] R. Wesdyk, Y.M. Joshi, J. De Vincentis, A.W. Newman, N.B. Jain, Int. J. Pharm. 93 (1993) 101–109.
[20] R. Wesdyk, Y.M. Yoshi, K. Morris, A. Newman, Int. J. Pharm. 65 (1990) 69–76.
[21] D.C. Zipperian, Ceram. Trans. 38 (1993) 631–640.
[22] J.C. Oppenheim, Microstruct. Sci. 17 (1989) 11–21.
[23] J. Krejei, J. Svejcar, J. Krejeova, O. Ambroz, D. Janova, K. Jioikovsky, Energy Technol. 5 (1998) 1497–1504.
[24] G.Q. Lu, K.C. Leong, Powder Technol. 81 (1994) 201–206.
[25] J. Krejcova, J. Brezina, O. Ambroz, J. Krejci, Prakt. Metallogr. 35 (1998) 71–79.
[26] H.F. Jang, A.G. Robertsson, R.S. Seth, J. Mat. Sci. 27 (1992) 6391–6400.
[27] J.A. Hunt, D.G. Vince, D.F. Williams, J. Biomed. Eng. 15 (1993) 39–45.
[28] J. Guicheux, O. Gauthier, E. Aguado, D. Heymann, P. Pilet, S. Couillaud, A. Faivre, G. Daculsi, J. Biomed. Mater. Res. 40 (1998) 560–566.
[29] B.I. Levy, J.B. Michel, J.L. Salzmann, P. Poitevin, M. Devissaguet, E. Scalbert, M.E. Safar, Am. J. Cardiol. 71 (1993) 8E–16E.
[30] J. Ryhanen, M. Kallioinen, J. Tuukkanen, J. Junila, E. Niemela, P. Sandvik, W. Serlo, J. Biomed. Mater. Res. 41 (1998) 481–488.
[31] F. Vazquez, S. Palacios, N. Aleman, F. Guerrero, Maturitas 25 (1996) 209–215.
[32] A. Hernandez, J.I. Calvo, P. Pradanos, L. Palacio, M.L. Rodriguez, J.A. de Saja, J. Membr. Sci. 137 (1997) 89–97.
[33] L. Zeman, L. Denault, J. Membr. Sci. 71 (1992) 221–231.
[34] M. Andersson, S. Folestad, J. Gottfries, M.O. Johansson, M. Josefson, K.-G. Wahlund, Anal. Chem. accepted (1999).
[35] L.L. Havlieck, R.D. Crain, Practical Statistics for the Physical Sciences, American Chemical Society, Washington, DC, 1988.
[36] P. Wnukowski, On the coating of particles in fluid-bed granulators, Ph.D. Thesis, Royal Institute of Technology, Stockholm, 1989.
[37] V.V. Nalimov, The Application of Mathematical Statistics to Chemical Analysis, Pergamon, Oxford, 1963.